Journal of Solid State Chemistry **146,** 329–335 (1999)
Article ID jssc.1999.8355, available online at http://www.idealibrary.com on IDEAL®

Glass Structure and Optical Nonlinearities in Thallium(I) Tellurium(IV) Oxide Glasses

B. Jeansannetas, S. Blanchandin, P. Thomas, P. Marchet, J. C. Champarnaud-Mesjard, T. Merle-Méjean, and B. Frit

Laboratoire de Matériaux Céramiques et Traitements de Surface, ESA CNRS 6015, 123 Avenue A. Thomas, 87060 Limoges Cédex, France

V. Nazabal, E. Fargin, and G. Le Flem

ICMCB, UPR CNRS 9048, Avenue du Dr Schweitzer, 33608 Pessac Cédex, France
E-mail: leflem@icmcb.u-bordeaux.fr

and

M. O. Martin, B. Bousquet, L. Canioni, S. Le Boiteux, P. Segonds, and L. Sarger

CPMOH, URA CNRS 283, Universite de Bordeaux 1, 351 Cours de la Libération, 33405 Talence Cédex, France

Received November 17, 1998; in revised form April 20, 1999; accepted May 7, 1999

The relationships between structure and nonlinear optical response at 1.5 μm in thallium(I) tellurite glasses are investigated. Usually in tellurite glasses, the introduction of a modifier ion changes the basic structural TeO_4 disphenoid entity progressively into a TeO_3 trigonal bipyramid via an intermediate TeO_{3+1} polyhedron. This evolution leads to a decrease of the nonlinear refractive index n_2. Nevertheless, if a modifier ion such as Tl^+ also has an ns^2 lone electron pair, n_2 increases although the same structural evolution is observed around the tellurium atoms. This result is related to the hyperpolarizability of the thallium oxygen entities, which has been evidenced by the structural study of both thallium(I) tellurite crystals and glasses of the same compositions. With this solid state chemistry approach, the highest nonlinear refractive index measured at 1.5 μm ($n_2 = 9.10^{-19}$ m²/W) and reported in oxide glasses has been obtained.

Key Words: **thallium(I) tellurite glasses; nonlinear index; glass structure.**

INTRODUCTION

The development of new glasses for photonic devices or communication systems in the near infrared region (1.3- or 1.5-μm communication wavelengths) requires the identification of the microscopic origin of the optical nonlinearities. Up to now the third-order nonlinearities were obtained by various techniques and at wavelengths (λ_m) more or less close to the fundamental absorption, leading to a puzzling discrepancy between values measured for the same material (1). Moreover, the resonant and nonresonant contributions are not always clearly isolated, and strong reduction of the $\chi(3)$ values is observed as λ_m increases. Recently accurate values of $\chi(3)$ were obtained at 1.5 μm for various metal oxides using a time-resolved interferometric technique (2). To be representative of a large scale of optical nonlinearities, the glasses were chosen on the basis of previous theoretical investigations analyzing the magnitude of the hyperpolarizability of ions and of more complex structural entities identified in such materials (3, 4). The largest nonlinear responses are generated by heavy cations having ns^2 electron pairs (Te^{4+}, Bi^{3+}, Pb^{2+}, Tl^+). In contrast, the lowest third-order nonlinearity in oxide glasses is found for the various forms of silica (1).

The origin of the nonlinearity in tellurite glasses was attributed to the Lewis $5s^2$ free doublet of tellurium (5). In the present study the attention is focused on the effect of a second lone pair holder (Tl^+ and/or Bi^{3+}) on the optical properties of tellurite glasses. This paper introduces the method of $\chi(3)$ measurement at 1.5 μm. It also describes the structural features characterizing the newly investigated glasses on the basis of the crystal chemistry of thallium(I) tellurites and discusses the relationships between the optical nonlinear response and the composition and structure of the glasses.

EXPERIMENTAL

(1) Preparation

The thallium tellurite glasses were prepared by melting various intimate mixtures of reagent grade TeO_2, Tl_2CO_3,

0022-4596/99 $30.00

and Bi_2O_3 in platinum crucibles for half an hour at 800°C. Tl_2CO_3 and Bi_2O_3 were commercial products (Aldrich, 99.9%) , and TeO_2 was prepared by decomposition of commercial H_6TeO_6 (Aldrich, 99.9%) at 550°C under flowing oxygen. The melts were quickly quenched by flattening between two brass blocks separated by a brass ring to obtain cylindrical samples 1.0 cm wide and 1.5 mm thick. The samples were then polished to obtain plane disks suitable for optical measurements ($\lambda/4$).

(2) Raman Spectra

The Raman spectra were recorded using a Dilor Z24 triple monochromator. The 514.5 nm emission line of a Spectra Physics ion laser (Model 2030) was used for excitation with incident power around 200 mW. Detection was done with a Hamatmasu cooled photomultiplier coupled with a photon-counting system. The spectral resolution was about 2 to 3 cm^{-1}.

(3) Measurement of the Nonlinear Index n_2

The nonlinear phase measurement relies on a Mach–Zehnder interferometer, as displayed in Fig. 1. The laser used in this setup is an OPO pumped by a TiSa oscillator (an OPAL and Tsunami from Spectra Physics), which delivers linearly polarized pulses of 150 fs (FWHM) at around 1.5 μm with peak power of 10 kW.

As the sample is located in the probe arm, the group index in the femtosecond regime at the operating wavelength is measured by simply using the delayed reference arm. When the (stronger) colinear pump beam interacts, the analysis of the interferometric signal gives access to both ultrafast and slow nonlinearities. An afocal lens in the probe arm provides a convenient beam waist in the sample, and great care is taken to ensure a perfect overlap between pump and probe beams. The signal from the two photodiodes $PD_{1,2}$ is used as an error signal to lock the average phase between the probe and reference beams and to measure the nonlinear phase shift induced by the electrooptically modulated pump beam (6). The resulting modulation of the signal is recorded using a spectrum analyzer. Absolute values and dynamics of the nonlinear susceptibilities can be measured through the evolution in amplitude and phase of the relevant Fourier component recorded as a function of the pump–probe delay.

As expected for purely nonresonant glass samples, the response arises from a pure instantaneous electronic contribution, and in the colinear configuration, this leads to a signal for which the average is due to the cross correlation between the pump and probe fields, and oscillations are due to third-order coupling processes. The maximum average phase shift, free from any coherent contributions, is related to the nonlinear index by

$$n_2 = \frac{\Delta\varphi\lambda\tau_p^2\sqrt{2}}{P_{pump}\,4\pi\arctan(l\lambda/2\pi W_0^2)}$$

(l is the length of the sample; $W_0 = 10$ μm is the beam waist into the sample; P_{pump} is the power pump beam; $\lambda = 1500$ nm; τ_p is the pump pulse duration).

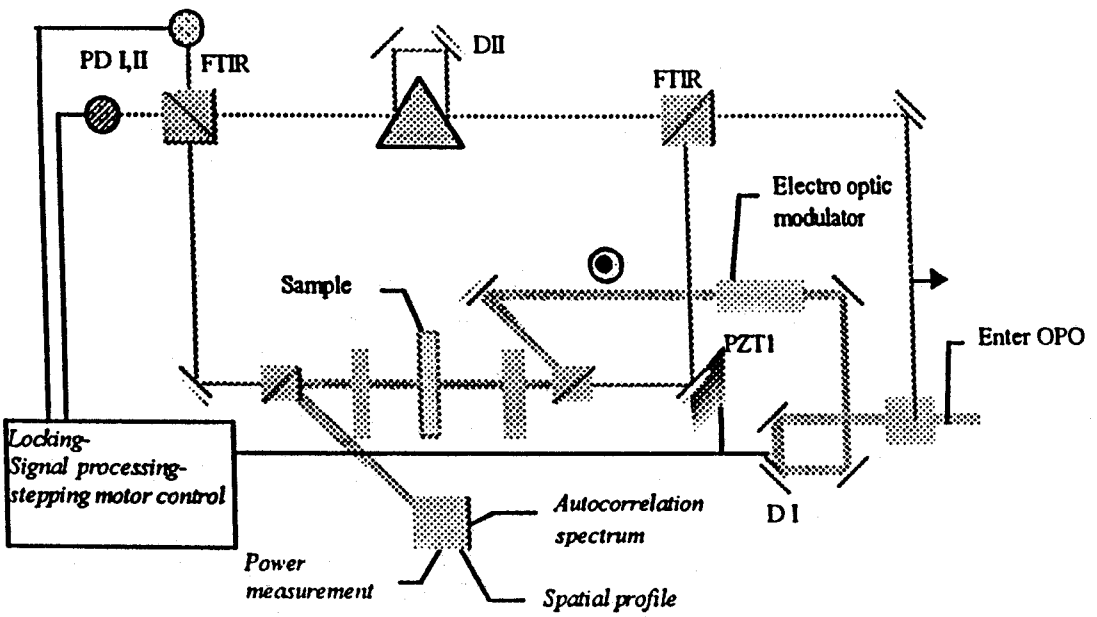

FIG. 1. Experimental set up used for the n_2 measurement (Ref. 2).

In this orthogonal pump-probe polarization scheme, the determination of χ_{xxyy} will be sufficient to characterize the nonlinear response, since the fourth-rank tensor is totally symmetric among its indices (i.e., $3^*\chi_{xxyy} = = 3^*\chi_{xyyx} = \chi_{xxxx}$) for isotropic materials.

The above linear relationship can be used to extract the sign, and as every parameter in this expression is carefully controlled, an absolute value of the instantaneous nonlinear refractive index can be computed. The accuracy of all optical parameters limits the precision of our measurements to roughly 10%. The sensitivity of this interferometer is around 10^{-20} m^2/W, mainly due to the moderate peak power of the OPO. As a typical example, the optical response of the SF6 glass is given in Fig. 2.

RESULTS

(1) Raman Spectra

Figure 3 compares the Raman spectra of glasses with compositions TeO_2, $Tl_2Te_3O_7$, and $Tl_2Te_2O_5$, with the spectrum of the crystalline phase $Tl_2Te_3O_7$. The Raman bands of the glass samples are broadened due to the distribution of interatomic bonds and angles in such disordered materials, but they overlap the peaks of the crystalline phase spectrum. The vibrations of the tellurium oxygen polyhedra are observed in the wavenumber range 450–800 cm^{-1}, with two strong bands peaking respectively at 650 and 430 cm^{-1}. Both bands are associated with shoulders appearing, respectively, at 750 and 460 cm^{-1}. Addition of Tl_2O leads to the appearance of new features: a strong band at about 710–720 cm^{-1} and a small one at about 250 cm^{-1}. The assignment will be discussed in the next paragraph.

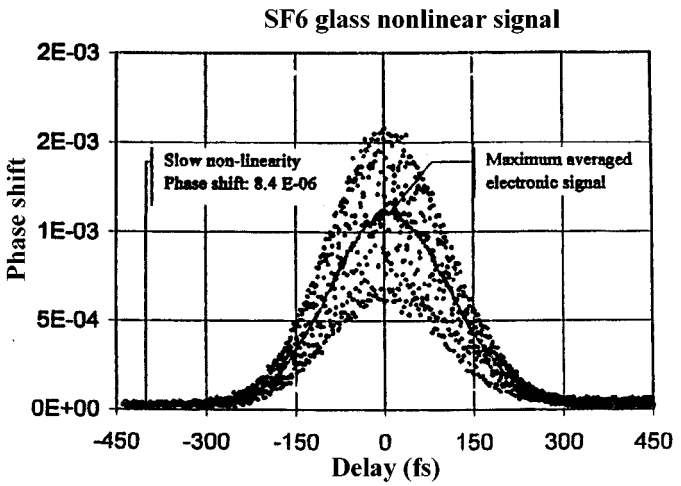

FIG. 2. Nonlinear response of the SF6 glass. The phase shift is given in radians (2).

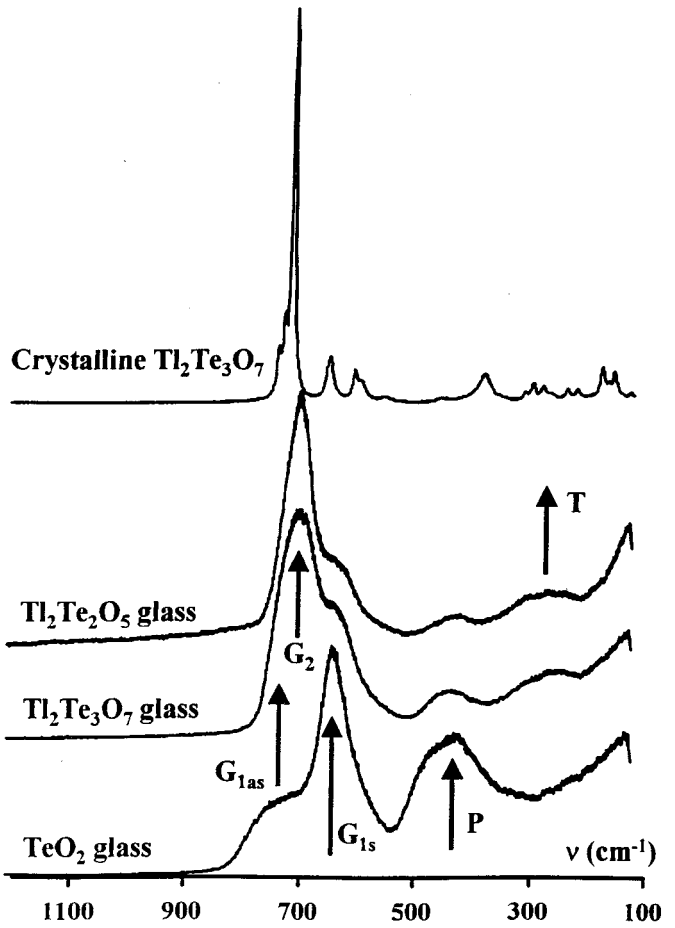

FIG. 3. Raman spectra of TeO_2, $Tl_2Te_3O_7$, and $Tl_2Te_2O_5$ glasses and of the $Tl_2Te_3O_7$ crystalline compound.

(2) Nonlinear Optical Measurement

The linear and nonlinear indexes of two selected thallium tellurite glasses and of one thallium-bismuth tellurite glass are reported in Table 1. To illustrate the influence of chemical composition, the linear and nonlinear indexes of various glasses were also measured at the same wavelength (1.5 μm).

All of the glasses exhibit perfect transmittance from the visible to the near IR. The cutoff wavelengths are far from the operating wavelength ($\lambda = 1.5$ μm) used for the refractive index measurements. Under these conditions the optical response can be considered a nonresonant phenomenon. In these oxides the highest linear or nonlinear indexes correspond to tellurite glasses. This result will be discussed in the next paragraph.

DISCUSSION

(1) Structure of Crystalline Tl–Te Mixed Oxides

The analogy between the Raman spectra of crystalline and vitreous forms of thallium(I) tellurium(IV) compounds

TABLE 1
Linear and Nonlinear Indexes, $\chi(3)$, at 1.5 μm for Various Glasses

Glasses (mol%)	n_0	n_2 (m^2/W) 10^{-19}	$\chi^{(3)}$ (V^2/m^2) 10^{-21}	Ref.
Herasil	1.467 ± 0.01	0.121 ± 0.09	0.046	2
Suprasil	1.422 ± 0.03	0.25 ± 0.2	0.089	2
86.5 $Ca(PO_3)_2$–13.5 Nb_2O_5	1.608 ± 0.05	0.18 ± 0.083	0.08	2
Borophosphate[a] 30 TiO_2	1.615 ± 0.03	1.33 ± 0.26	0.61	2
Borophosphate[a] 30 Nb_2O_5	1.772 ± 0.03	2.06 ± 0.25	1.14	2
SF59	1.880 ± 0.02	4.50 ± 0.50	2.82	2
SF6	1.788 ± 0.01	2.15 ± 0.23	1.20	2
90 TeO_2–10 Al_2O_3	2.003 ± 0.06	5.38 ± 1.19	3.81	2
90 TeO_2–10 Nb_2O_5	2.144 ± 0.03	6.93 ± 0.72	5.63	2
85 TeO_2–15 Nb_2O_5	2.145 ± 0.05	6.41 ± 0.93	5.21	2
80 TeO_2–20Nb_2O_5	2.155 ± 0.05	5.94 ± 0.81	4.93	2
82 TeO_2–18 Tl_2O	2.125 ± 0.02	8.60 ± 1.0	6.87	2
79 TeO_2–21 Tl_2O	2.094 ± 0.02	8.90 ± 1.0	6.90	2
85 TeO_2–13.5 Tl_2O–1.5 Bi_2O_3	2.156 ± 0.07	9.10 ± 1.7	7.48	2

[a] Borophosphate = 95$NaPO_3$–5$Na_2B_4O_7$ (mol%).

implies a nearly identical structural arrangement of oxygen around the metallic ions. In this context, some important points emerge from a careful analysis of the structures of the various crystalline phases observed within the Tl_2O–TeO_2 system, i.e., α- and β-TeO_2, $Tl_2Te_3O_7$, α-$Tl_2Te_2O_5$, Tl_2TeO_3, and Tl_2O (Tables 2 and 3) (7–13).

(i) In each structure the arrangement of anions around cations is highly anisotropic and characteristic of strong stereochemical activity of the electron lone pairs E of the cations.

(ii) From TeO_2 to Tl_2TeO_3, the anionic coordination polyhedron of Te^{4+} changes progressively from a TeO_4 disphenoid (in fact a TeO_4E trigonal bipyramid with two "relatively long" axial distances, two "relatively short" equatorial distances, and the lone pair E so directed as to constitute the third equatorial corner (Fig. 4a) to a TeO_3 trigonal pyramid (in fact a TeO_3E tetrahedron (Fig. 4c) via an intermediate TeO_{3+1} polyhedron (Fig. 4b). The anionic polyhedra of Tl^+ cations show nearly the same kind of evolution with a progressive transformation of the TlO_4E trigonal bipyramids observed in $Tl_2Te_3O_7$ (Fig. 4e) into the perfect TlO_3E tetrahedra of Tl_2O (Fig. 4d). Such evolutions clearly indicate that increasing thallium content enhances the anisotropic character of the anionic arrangement around cations and that the stereochemical activity of the lone pair of tellurium atoms is strengthened by the presence of a second lone pair holder.

(iii) TeO_4E polyhedra are systematically connected via Te–^{eq}O–^{ax}–Te bridges, which can be single bridges (corner–sharing) or double bridges (edge-sharing).

(2) Analysis of the Raman Spectra of Thallium(I) Tellurite Glasses

On the basis of the above structural observations and of the analysis of the Raman spectra of homologous crystalline phases (14, 15), the Raman spectra of Tl_2O–TeO_2 glasses (see Fig. 3) can be interpreted as follows (Table 4). The spectrum of the pure TeO_2 glass is mainly constituted of two wide, asymmetric bands at about 650 and 430 cm^{-1}.

TABLE 2
The Tellurium Coordination Polyhedra and Their Linking in Crystalline α and β-TeO_2 and Tl–Te Mixed Oxides

	TeO_x Polydedra	Te–O Distances (Å)	TeO_x Linking	Ref.
α-TeO_2	TeO_4	2 × 2.12; 2 × 1.88	3-D: corner-sharing TeO_4	8
β-TeO_2	TeO_4	1.87/1.89/2.07/2.15	2-D: edge and corner-sharing TeO_4	9
$Tl_2Te_3O_7$	$Te(2)O_3$	1.837/1.898/1.912	Te_3O_7 strips: edge and corner-sharing polyhedra	10
	$Te(1)O_{3+1}$	1.833/1.912/2.032/2.223		
	$Te(3)O_4$	1.834/1.943/2.108/2.154		
α-$Tl_2Te_2O_5$	$Te(2)O_{3+1}$	1.870/1.873/2.041/2.327	Te_2O_5 sheets: edge and corner-sharing polyhedra	11
	$Te(1)O_4$	1.908/1.925/2.034/2.162		
Tl_2TeO_3	TeO_3	1.826/1.828/1.891	Isolated TeO_3 groups	12

TABLE 3
The Thallium Coordination Polyhedra and Their Linking in Crystalline Tl_2O and Tl–Te Mixed Oxides

	TlO_x Polyhedra	Tl–O Distances (Å)	TlO_x Linking	Ref.
$Tl_2Te_3O_7$	$Tl(1)O_4$	2.471/2.588/2.700/2.828	Tl_2O_4 chains: edge-sharing polyhedra	10
	$Tl(2)O_4$	2.488/2.652/2.736/2.942		
α-$Tl_2Te_2O_5$	$Tl(1)O_4$	2.580/2.584/2.646/2.840	Tl_2O_4 chains: face and corner-sharing polyhedra	11
	$Tl(2)O_4$	2.681/2.775/2.799/2.813		
Tl_2TeO_3	$Tl(1)O_3$	2.447/2.745/2.831	Tl_2O_3 sheets: edge and corner-sharing polyhedra	12
	$Tl(2)O_4$	2.492/2.615/2.653/2.910		
Tl_2O	$Tl(1)O_3$	3×2.517	Tl_2O sheets: edge and corner-sharing polyhedra	13
	$Tl(2)O_3$	3×2.539		

The first, at 650 cm^{-1} (denoted G_{1s}), can be assigned to the totally symmetrical stretching vibration of the pseudo-molecular TeO_2 entity of the TeO_4 polyhedron (short equatorial bonds) and its shoulder (denoted G_{1as}) to the corresponding asymmetrical vibrations. The peak at 430 cm^{-1} (denoted P) and its shoulder at about 460 cm^{-1} can be assigned to the stretching vibrations of, respectively, the single and double Te–^{eq}O–^{ax}Te bridges.

Addition of Tl_2O leads to the appearance of two new bands, an intense one at about 710–720 cm^{-1} and a weak one at about 250 cm^{-1}, related to a progressive decrease of the intensity of the G_{1s} and P peaks. With respect to the Raman spectra of crystalline phases (14, 15) and to the previous results of Sekyia *et al.* (16) and Dexpert-Ghys *et al.* (17) on TeO_2-based glasses, the peak at 710–720 cm^{-1} (called G_2) has been assigned to the symmetric stretching vibrations of isolated TeO_3 groups. The peak at 250 cm^{-1}, which is not observed for pure TeO_2 glass, could be assigned to Tl–O vibrations.

With increasing Tl content,

(i) the relative intensity of the G_{1s} peak decreases, and the ratio G_2/G_{1s} increases; and

(ii) the ratios P/G_{1s} and $P/(G_{1s} + G_2)$, which determine the relative quantities of Te–O–Te linkages with respect to TeO_3, TeO_{3+1}, or TeO_4 entities, decrease.

Such an evolution clearly indicates a progressive transformation of corner- and/or edge-sharing TeO_4 polyhedra into isolated TeO_3 trigonal pyramids. Therefore, thallium tellurite glasses are probably formed of TeO_x ($4 \leq x \leq 3$) structural units linked together both by single and double Te–^{eq}O–^{ax}Te bridges. As observed for the corresponding crystalline phases, increasing thallium content leads to a depolymerization of the tellurium structural units framework due to both the transformation of TeO_4 entities into isolated TeO_3 polyhedra and the decrease of the number of Te–O–Te linkages.

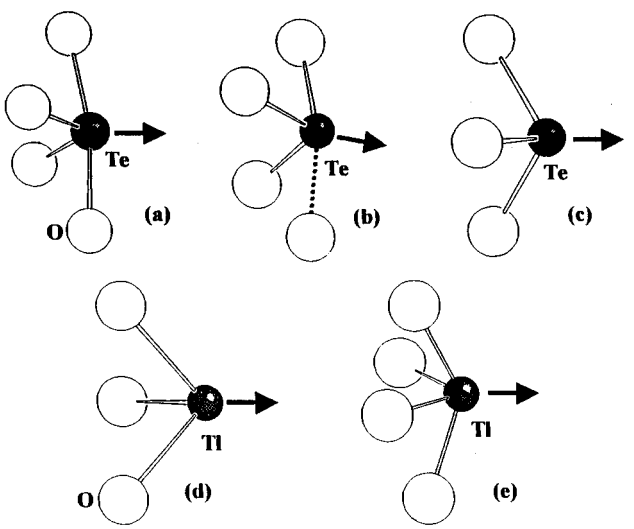

FIG. 4. The various cation coordination polyhedra observed in crystalline Tl–Te mixed oxides (arrows visualize the direction toward which the lone pairs E are directed).

TABLE 4
Decomposition of the Raman Spectra peaks of TeO_2, $Tl_2Te_3O_7$, and $Tl_2Te_2O_5$ Glasses and Crystalline $Tl_2Te_3O_7$

Peaks (cm^{-1})	Assignment	Relative Intensity Ratio
TeO_2 glass		
747	G_{1as} : TeO_4	
641	G_{1s} : TeO_4	
450	P : Te–O–Te	$P/G_{1s} = 0.60$
$Tl_2Te_3O_7$ glass		
710	G_2 : TeO_3 and/or TeO_{3+1}	
636	G_{1s} : TeO_4	$G_2/G_{1s} = 1.21$
450	P : Te–O–Te	$P/(G_{1s} + G_2) = 0.06$
$Tl_2Te_2O_5$ glass		
709	G_2 : TeO_3 and/or TeO_{3+1}	
637	G_{1s} : TeO_4	$G_2/G_{1s} = 2.27$
450	P : Te–O–Te	$P/(G_{1s} + G_2) = 0.03$
Crystalline $Tl_2Te_3O_7$		
743	TeO_3	
600–650	TeO_{3+1} and/or TeO_4	
400	Te–O–Te	

TABLE 5
Variation of the Nonlinear Index Vs Cation Concentration

Glass composition (mol%)	Densities (g/cm^3)	Te Concentration (10^{22} at./cm^3)	(Al, Nb, Tl) concentration (10^{22} at./cm^3)	n_2/n_2SF59 1.5 μm	n_2/n_2SF59 0.8 μm	Ref.
SF59				4.5[a]	10[a]	20
$90TeO_2$–$10Al_2O_3$	5.01	1.79	0.39	1.2	1.8	5
$85TeO_2$–$15Al_2O_3$	4.99	1.69	0.60		1.2	5
$80TeO_2$–$20Al_2O_3$	5.03	1.64	0.82		1.1	5
$95TeO_2$–$5Nb_2O_5$	5.52	1.91	0.10		2.1	20
$90TeO_2$–$10Nb_2O_5$	5.40	1.72	0.38	1.5	1.9	2,20
$85TeO_2$–$15Nb_2O_5$	5.34	1.56	0.55	1.4	1.8	2,20
$80TeO_2$–$20Nb_2O_5$	5.20	1.39	0.69	1.3	1.8	2,20
82 TeO_2–18 Tl_2O	6.43	1.55	0.66	1.9		2
79 TeO_2–21 Tl_2O	6.59	1.45	0.78	2.0		2

[a] n_2 SF59 in 10^{-19} m^2/W.

(3) Relationship Between Glass Composition and Nonlinear Optical Properties

As shown by the values of Table 1, the nonlinear indices of tellurite glasses are the highest found for oxide glasses. The values depend on both the concentration and the nature of the countercation introduced into the TeO_2 glassy matrix. The influence of these two crucial parameters emerges from the data reported in Table 5.

For all these glasses, structural analyses have unambiguously shown (this work and (5)) that the introduction of additional cations (Al^{3+}, Nb^{5+}, Tl^+), which obviously corresponds to a decrease in the tellurium concentration, leads to the progressive transformation of TeO_4 disphenoids into TeO_3 trigonal pyramids through an intermediate TeO_{3+1} asymmetric polyhedron. A theoretical approach to this phenomenon was carried out through ab initio calculations (18). For the $(TeO_4)^{4-}$ and $(TeO_3)^{2-}$ groups, it led to the two molecular diagrams of Figs. 5 and 6. In both cases, the highest occupied molecular orbital (3a1) is of the antibonding type. It results essentially from a combination of the tellurium 5*s* atomic orbital and the oxygen 2*p* atomic orbital and is hence strongly correlated with the $5s^2$ lone pair of tellurium. The corresponding electrons are highly polarizable and are therefore mainly responsible for the macroscopic high linear and nonlinear indices. Polarizabilities have been calculated by a perturbative treatment where this 3a1 orbital is coupled by external field perturbation to the three antibonding orbitals: the mean polarizability α was found to be about 20% higher for the $(TeO_4)^{4-}$ cluster than for the $(TeO_3)^{2-}$ cluster (45.3 and 35.8 u.a., respectively). The pertinence of such a result was confirmed by calculating the linear index of a pure TeO_2 glass containing only TeO_4 groups using the Clausius–Mossoti relationship $(n_0^2 - 1)/(n_0^2 + 2) = N\alpha/3\varepsilon_0$, where N is the volumetric concentration of the TeO_4 entities, n_0 the linear index, and ε_0 the permittivity of free space. From this equation, n_0 is estimated to be 2.3, a value which is close to the 2.1 to 2.2 values observed for the glasses richest in tellurium.

Therefore, it can be concluded that the addition of increasing quantities of modifying oxides to a TeO_2 glassy matrix should result in a decrease in n_2. This is acutally observed for Nb_2O_5 glasses and still more clearly for Al_2O_3 glasses, but not at all for Tl_2O glasses. The reason for such a discrepancy is an increasing contribution to the nonlinear response of the added cations from Al^{3+} to Tl^+.

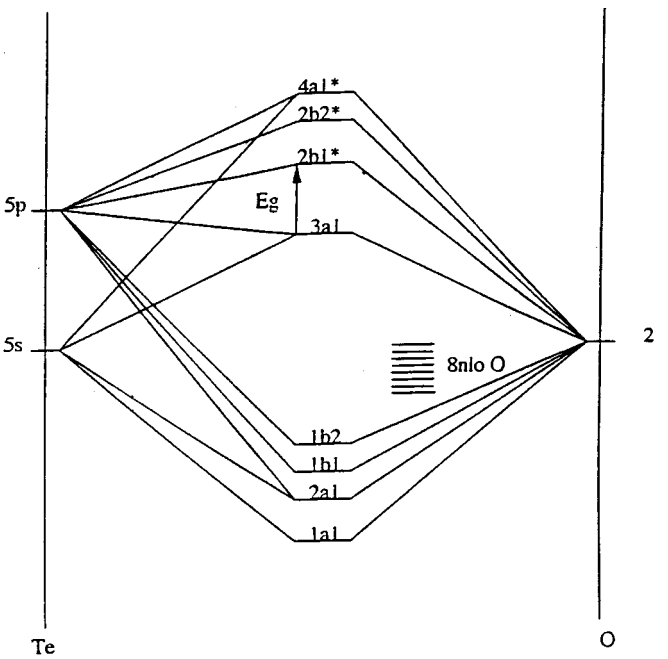

FIG. 5. Molecular orbital diagram of $[TeO_4]^{4-}$ entity. (nloO: nonbonding orbital of oxygen atoms; E_g is the energy difference between homo and lumo states) (5).

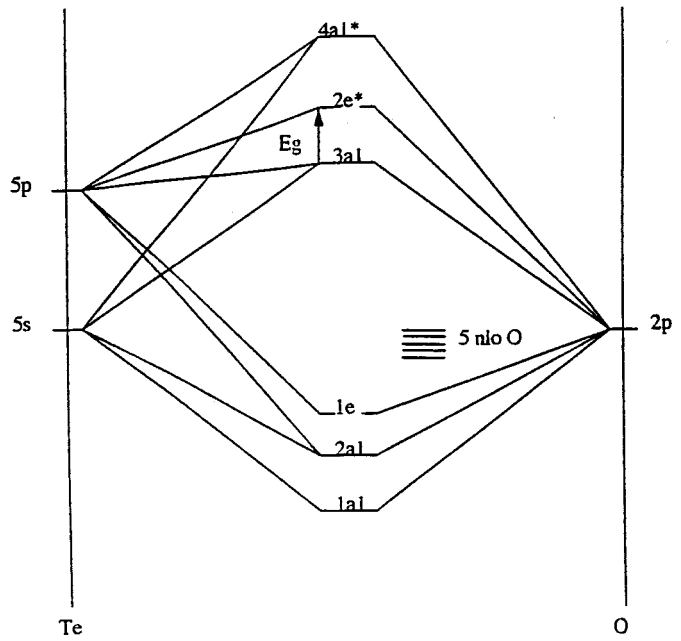

FIG. 6. Molecular orbital diagram of $[TeO_3]^{2-}$ entity. (nloO: nonbonding orbital of oxygen atoms; E_g is the energy difference between homo and lumo states) (5).

Indeed, even with lower tellurium concentrations, Nb_2O_5 glasses exhibit higher n_2 values than Al_2O_3 glasses. This phenomenon has been analyzed in the context of the bond orbital theory and the increased polarization of the Nb–O bond with increasing p–d orbital overlap evidenced (19).

As for the Tl_2O glasses investigated, although they contain the lowest Te content and were subjected to the same structural evolution around the tellurium atoms, they exhibit the highest n_2 values. Such behavior is surely related to the high stereochemical activity of the lone pair E of thallium atoms, which allows strong polarizability of all of the thallium–oxygen entities.

CONCLUSION

In conclusion, nonresonant nonlinearities can be predicted in oxide glasses by analyzing the respective effects of high-valence transition-metal ions such as Ti(IV) and Nb(V) and highly polarizable ions such as Te(IV), Tl(I), and Bi(III). The reported n_2 values can be correlated with the electronic polarizability (or hyperpolarizability) of individual metal oxygen entities in connection with the structural features of short-range order appearing in the glasses. In such oxide glasses the upper limit of nonresonant n_2 is about 10^{-18} m^2/W. As mentioned in the Introduction, the lower limits of n_2 for oxide glasses are provided by the various forms of silica. Only the introduction of fluorine in glasses can decrease n_2. In contrast the addition of d^0 shell metal ions like Ti^{4+} or Nb^{5+} or metal ions with lone pairs such as Te^{4+}, Tl^+, or Bi^{3+} increases the nonlinear response. Theoretical approaches connected with the identification of the structural groups in the glasses allow an explanation for the magnitude of the nonlinear index.

ACKNOWLEDGMENT

B. Jeansannetas thanks the "Conseil Regional du Limousin" for financial support.

REFERENCES

1. E. M. Vogel, M. J. Weber, and E. M. Krol, *Phys. Chem. Glasses* **32,** 231 (1991).
2. L. O. Canioni, M. O. Martin, B. Bousquet, and L. Sarger, *Opt. Commun.* **151,** 241 (1998).
3. E. Fargin, A. Berthereau, T. Cardinal, J. J. Videau, A Villesuzanne, and G. Le Flem, *Ann. Chim. Sci Mater.* **23,** 27 (1998).
4. S. Le Boiteux, P. Segonds, L. Canioni, L. Sarger, T. Cardinal, C. Duchesne, E. Fargin, and G. Le Flem, *J. Appl. Phys.* **81**(3), 1481 (1997).
5. A. Berthereau, E. Fargin, A. Villesuzanne, R. Olazcuaga, G. Le Flem, and L. Ducasse, *J. Solid State Chem.* **126,** 143 (1996).
6. L. Sarger, P. Segonds, L. Canioni, F. Adamietz, A. Ducasse, C. Duchesne, E. Fargin, R. Olazcuaga, and G. Le Flem, *J. Opt. Soc. Amer. B.* **11**(6), 995 (1994).
7. B. Jeansannetas, P. Marchet, P. Thomas, J. C. Champarnaud-Mesjard, and B. Frit, *J. Mater. Chem.* **8**(4), 1039 (1998).
8. P. A. Thomas, *J. Phys. C Solid State Phys.* **21,** 4611 (1988).
9. H. Beyer, *Z. Kristallogr.* **124,** 228 (1967).
10. B. Jeansannetas, P. Thomas, J. C. Champarnaud-Mesjard and B. Frit, *Mater. Res. Bull.* **32**(1), 51 (1997).
11. B. Jeansannetas, P. Thomas, J. C. Champarnaud-Mesjard, and B. Frit, *Mater. Res. Bull*, to be published.
12. B. Frit and D. Mercurio, *Rev. Chim. Min.* **17,** 192 (1980).
13. H. Sabrowsky, *Z. Anorg. Allg. Chem.* **381,** 266 (1971).
14. B. Jeansannetas, Thesis, University of Limoges, (1998).
15. T. Merle-Méjean, A. Mirgorodsky, B. Jeansannetas, P. Thomas, J. C. Champarnaud-Mesjard, and B. Frit, *J. Phys. Chem. Solids*, in press.
16. T. Sekiya, N. Mochida, A. Ohtsuka, and M. Tonokawa, *J. Non-Cryst. Solids* **144,** 128 (1992).
17. J. Dexpert-Ghys, B. Piriou, S. Rossignol, J. M. Reau, B. Tanguy, J. J. Videau, and J. Portier, *J. Non-Cryst. Solids* **170,** 167 (1994).
18. E. Fargin, A. Berthereau, T. Cardinal, G. Le Flem, L. Ducasse, L. Canioni, P. Segonds, and A. Ducasse, *J. Non-Cryst. Solids* **203,** 96 (1996).
19. T. Cardinal, E. Fargin, G. Le Flem, and S. Le Boiteux, *J. Non-Cryst. Solids* **222,** 228 (1997).
20. A. Berthereau, Y. Le Luyer, R. Olazcuaga, G. Le Flem, M. Couzi, L. Canioni, P. Segonds, L. Sarger, and A. Ducasse, *Mater. Res. Bull.* **29**(9), 933 (1994).